2011

Volatility and High Thermal Stability in Mid to Late First Row Transition Metal Diazadienyl Complexes

Thomas J Knisley, *Wayne State University*

ORGANOMETALLICS

ARTICLE

pubs.acs.org/Organometallics

Volatility and High Thermal Stability in Mid- to Late-First-Row Transition-Metal Diazadienyl Complexes

Thomas J. Knisley,[†] Mark J. Saly,[‡] Mary Jane Heeg,[†] John L. Roberts,[§] and Charles H. Winter*[,†]

[†]Department of Chemistry, Wayne State University, Detroit, Michigan 48202, United States

[‡]SAFC Hitech, 1429 Hilldale Avenue, Haverhill, Massachusetts 01832, United States

[§]SAFC Hitech, Power Road, Bromborough, Wirral CH62 3QF, U.K.

Supporting Information

ABSTRACT: Treatment of MCl_2 (M = Cr, Mn, Fe, Co, Ni) with 2 equiv of lithium metal and 1,4-di-*tert*-butyl-1,3-diazadiene (^{tBu2}DAD) in tetrahydrofuran at ambient temperature afforded Cr(^{tBu2}DAD)$_2$ (38%), Mn(^{tBu2}DAD)$_2$ (81%), Fe(^{tBu2}DAD)$_2$ (47%), Co(^{tBu2}DAD)$_2$ (36%), and Ni(^{tBu2}DAD)$_2$ (41%). Crystal structure determinations revealed monomeric complexes that adopt tetrahedral coordination environments and were consistent with ^{tBu2}DAD radical anion ligands. To evaluate the viability of M(^{tBu2}DAD)$_2$ (M = Cr, Mn, Fe, Co, Ni) as potential film growth precursors, thermogravimetric analyses, preparative sublimations, and solid-state decomposition studies were performed. Mn(^{tBu2}DAD)$_2$ is the most thermally robust among the series, with a solid-state decomposition temperature of 325 °C, a sublimation temperature of 120 °C/0.05 Torr, and a nonvolatile residue of 4.3% in a preparative sublimation. Thermogravimetric traces of all complexes show weight loss regimes from 150 to 225 °C with final percent residues at 500 °C ranging from 1.5 to 3.6%. Thermolysis studies reveal that all complexes except Mn(^{tBu2}DAD)$_2$ decompose into their respective crystalline metal powders under an inert atmosphere. Mn(^{tBu2}DAD)$_2$ may afford amorphous manganese metal upon thermolysis.

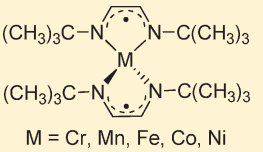

INTRODUCTION

Thin films containing the mid- to late-first-row transition metals have many important existing and future applications.[1,2] In the microelectronics area, copper has replaced aluminum as the interconnect material in integrated circuits due to its lower resistivity and higher resistance to electromigration.[1] Ultrathin (2−8 nm) manganese−silicon−oxygen layers have been proposed as replacements for existing nitride-based copper diffusion barrier layers in future devices.[3] Since copper does not nucleate well on SiO_2 and other surfaces,[1] it is difficult to deposit copper metal into the surface features of microelectronics substrates. Accordingly, there has been considerable interest in the formation of seed layers of metals such as chromium, cobalt, and others which adhere better to substrates, and upon which copper films can be subsequently grown.[4] Nickel and nickel silicide (NiSi) are important contact materials in device fabrication.[5] Magnetoresistive random access memory devices require the growth of thin, conformal layers of magnetic metals such as nickel, cobalt, and iron.[6] Microelectronics device dimensions are scheduled to reach 22 nm by 2012, and existing deposition processes will soon not be able to provide the required level of thickness control and conformality, especially in high aspect ratio features.[1,7] The atomic layer deposition (ALD) film growth method is well-suited for nanoscale film growth, since it affords inherently conformal coverage and subnanometer film thickness control, due to its self-limited growth mechanism.[8] In a typical ALD process, a metal precursor is transported in the vapor phase by an inert carrier gas into the reaction chamber, where it chemisorbs upon substrate surface reactive sites. Once all accessible surface reactive sites have become occupied, the surface is saturated, no further reactions can occur, and unreacted precursor and reaction byproducts are removed from the reactor with an inert gas purge. At this point, a second precursor vapor is passed over the substrate, which reacts with the surface-adsorbed metal precursors to produce the desired thin film material. To conclude a growth cycle, a second inert gas purge is then performed to remove additional byproducts and excess precursor. The growth rate per cycle generally remains constant, allowing the film thickness to be dependent only upon the number deposition cycles.

ALD precursors must combine high thermal stability, high reactivity toward a second reagent to afford the desired thin film material, and enough volatility to permit vapor transport at temperatures of generally <200 °C.[9] Thermal decomposition of the precursor within the deposition chamber would lead to loss of the self-limited ALD growth mechanism and uncontrolled chemical vapor deposition (CVD) like film growth. Among the first-row transition elements, ALD processes are best developed for copper metal,[2] and precursors have incorporated amidinate, β-diketonate, β-ketoiminate, β-diketonate, alkoxide, and chloride ligands. Reducing agents have included molecular hydrogen, main-group-metal alkyls, alkylsilanes, alcohols containing β-hydrogen atoms, formic acid, and zinc metal.[2] In addition, plasma activation has been used to get around the low reactivities

Received: July 12, 2011
Published: August 25, 2011

dx.doi.org/10.1021/om200626w | *Organometallics* 2011, 30, 5010–5017

Chart 1. Possible Forms of α-Diimine Ligands

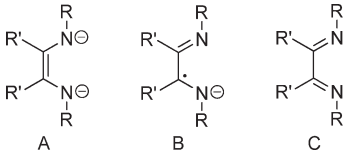

of the precursors toward many of the reducing agents.[2b,m] ALD precursors for nickel metal growth have employed amidinate, alkoxide, and cyclopentadienyl ligands, and reducing coreagents have included ammonia plasma, hydrogen plasma, and molecular hydrogen.[2o,5] Growth of cobalt metal films by ALD has employed precursors containing cyclopentadienyl, amidinate, and carbonyl ligands.[10] Reducing coreagents include ammonia plasma, hydrogen plasma, and nitrogen plasma. ALD growth of iron metal on aerogels was claimed,[11] although no details were given. Manganese and chromium metal films have not been grown by ALD. Existing ALD precursors for copper, nickel, and cobalt generally suffer from low thermal stability, low reactivity toward reducing agents, or a combination of both.[2,5,10] Use of plasmas can overcome the low reactivities toward reducing agents, but plasma reactors are more complex than thermal reactors and plasmas can introduce undesired damage to the films.

Nitrogen ligands are of special interest in the design of ALD precursors, since the metal−nitrogen bonds are often highly reactive. However, the challenge is to identify nitrogen ligands that can also lead to volatile and highly thermally stable complexes. Recently, 1,4-diaza-1,3-butadienes (RN=CR′CR′=NR, R = alkyl, aryl, R′ = H, alkyl) have been investigated as ligands, especially for the mid- to late-first-row transition metals.[12−16] These ligands are redox noninnocent and can exist in three distinct forms (Chart 1).[13−16] Form A is formally dianionic and has a short carbon−carbon distance and long carbon−nitrogen distances, form B is a monoanionic, delocalized radical anion with intermediate carbon−carbon and carbon−nitrogen distances, and form C is neutral with a long carbon−carbon distance and short carbon−nitrogen distances. These ligands can form square-planar to distorted-tetrahedral complexes with chromium(II),[13] manganese(II),[14] iron(II),[15] cobalt(II),[16] and nickel(II) ions.[16]

Our long-term research objective is to develop new ALD precursors and processes that afford thin films of high-purity chromium, manganese, iron, cobalt, nickel, and copper metal thin films. These processes should obey the self-limited ALD growth mechanism over the widest possible temperature range to meet future microelectronics and other manufacturing requirements. To meet these goals, highly volatile precursors with the highest possible thermal stabilities are required. 1,4-Diaza-1,3-butadiene-derived ligands form four-coordinate complexes with the mid- to late-transition-metal ions in the +2 oxidation state,[13−16] and the nature of the nitrogen and carbon substituents should be easily modified to adjust volatility, thermal stability, and reactivity. Herein we report the synthesis, structure, volatility, thermal stability, and thermal decomposition of a series of chromium(II), manganese(II), iron(II), cobalt(II), and nickel(II) complexes that contain 1,4-di-*tert*-butyl-diaza-1,3-butadienyl (^{tBu2}DAD) ligands. These complexes sublime at low temperatures, have high solid-state decomposition temperatures, decompose to the metals upon heating, and may serve as precursors in ALD and other film growth procedures that require molecular precursors.

Table 1. Crystal Data and Data Collection Parameters for 1 and 3−5

	1	3	4	5
formula	$C_{20}H_{40}CrN_4$	$C_{20}H_{40}FeN_4$	$C_{20}H_{40}CoN_4$	$C_{20}H_{40}NiN_4$
fw	388.56	392.41	395.49	395.27
space group	$P\bar{1}$	*Pnma*	*Pnma*	*Pnma*
a (Å)	11.1969(10)	18.3813(8)	18.2363(8)	18.1617(7)
b (Å)	14.0988(13)	13.4195(6)	13.3810(6)	13.3739(5)
c (Å)	14.4001(14)	9.2799(4)	9.2410(4)	9.2280(4)
α (deg)	86.857(2)			
β (deg)	82.672(3)			
γ (deg)	88.077(3)			
V (Å^3)	2250.5(4)	2289.05(17)	2254.99(17)	2241.41(15)
Z	4	4	4	4
T (K)	100(2)	100(2)	100(2)	100(2)
λ (Å)	0.71073	0.71073	0.71073	0.71073
ρ_{calcd} (g cm^{-3})	1.147	1.139	1.165	1.171
μ (mm^{-1})	0.518	0.668	0.770	0.875
$R(F)$ (%)[a]	6.65	2.96	2.62	3.02
$R_w(F)$ (%)[a]	16.83	7.78	6.64	7.72

[a] $R(F) = \Sigma||F_o| - |F_c||/\Sigma|F_o|$; $R_w(F) = [\Sigma w(F_o^2 - F_c^2)^2/\Sigma w(F_o^2)^2]^{1/2}$, for $I > 2\sigma(I)$.

RESULTS AND DISCUSSION

Synthesic Aspects. Treatment of anhydrous metal(II) chlorides (MCl_2, M = Cr, Mn, Fe, Co, Ni) with 2 equiv of 1,4-di-*tert*-butyl-diaza-1,3-butadiene and 2 equiv of lithium metal afforded complexes of the formula M(^{tBu2}DAD)$_2$ as purple (**1**), black (**2**), brown (**3**), blue (**4**), and dichroic red/green (**5**) crystalline powders (eq 1). Crystalline samples of **1**−**5** were subsequently obtained by either sublimation or crystallization in hexane at −23 °C. The synthetic procedure is a modification of previous routes to transition-metal complexes containing 1,4-diaza-1,3-butadiene ligands.[13−16] It was not possible to prepare any copper(II) or copper(I) complexes containing ^{tBu2}DAD ligands, since all reactions afforded copper powders. The compositions of **1**−**5** were determined by a combination of analytical and spectroscopic techniques and by X-ray crystal structure determinations of **1** and **3**−**5**. Complex **5** is the only diamagnetic species in the series and revealed *tert*-butyl and imino hydrogen atom resonances at *δ* 1.93 and 8.95, respectively, in the ^{1}H NMR spectrum in benzene-d_6. In the infrared spectra of **1**−**5**, the carbon−nitrogen stretching frequencies were observed between 1716 and 1698 cm^{-1}. Solid-state magnetic moments for **1**−**4** were 2.83, 3.85, 2.88, and 1.75 μ_B, respectively. Very similar values were measured in benzene solution using the Evans method, suggesting similar molecular structures in the solid state and solution. The magnetic moments for **1**−**4** are very close to those expected for high-spin M(II) ions that are antiferromagnetically coupled to two unpaired electrons of radical anion ^{tBu2}DAD ligands (Chart 1, form B). Analogous magnetic coupling is well-established in transition-metal complexes containing 1,4-diaza-1,3-butadiene radical anion ligands with various alkyl and aryl substituents.[12−16] Complexes **3**[15e] and **5**[16e] have been previously reported, and **4** was studied theoretically.[16g] The

Table 2. Selected Bond Lengths (Å) and Angles (deg) for 1

Cr(1)−N(1)	1.924(3)	C(1)−C(2)	1.395(4)
Cr(1)−N(2)	1.924(2)	C(11)−C(12)	1.337(5)
Cr(1)−N(3)	1.928(3)	C(1)−N(1)	1.360(4)
Cr(1)−N(4)	1.934(2)	C(2)−N(2)	1.356(4)
Cr(1)−C(1)	2.351(3)	C(11)−N(3)	1.386(4)
Cr(1)−C(2)	2.361(3)	C(12)−N(4)	1.367(4)
N(1)−Cr(1)−N(2)	91.79(11)	N(3)−Cr(1)−N(4)	82.91(11)
N(1)−Cr(1)−N(3)	127.13(11)	Cr(1)−N(1)−C(1)	89.69(19)
N(1)−Cr(1)−N(4)	118.60(11)	Cr(1)−N(2)−C(2)	90.38(18)
N(2)−Cr(1)−N(3)	123.99(11)	Cr(1)−N(3)−C(11)	112.1(2)
N(2)−Cr(1)−N(4)	114.94(11)	Cr(1)−N(4)−C(12)	112.2(2)

Table 3. Selected Bond Lengths (Å) and Angles (deg) for 3−5

	3	4	5
M−N(1)	1.952(1)	1.929(1)	1.919(1)
M−N(2)	1.956(1)	1.936(1)	1.916(1)
M−N(3)	1.953(1)	1.931(1)	1.917(1)
C(1)−C(2)	1.393(2)	1.393(2)	1.401(2)
C(9)−C(9)′	1.397(2)	1.403(2)	1.407(2)
C(1)−N(1)	1.339(2)	1.334(2)	1.326(2)
C(2)−N(2)	1.341(2)	1.332(2)	1.326(2)
C(9)−N(3)	1.347(1)	1.335(2)	1.330(1)
N(1)−M−N(2)	84.72(5)	84.65(6)	83.51(5)
N(1)−M−N(3)	122.74(3)	122.93(4)	123.93(3)
N(2)−M−N(3)	123.28(3)	123.26(4)	123.62(3)
N(3)−M−N(3)′	85.00(5)	84.77(6)	83.65(5)
M−N(1)−C(1)	110.18(10)	110.76(11)	112.33(10)
M−N(2)−C(2)	109.97(9)	110.61(11)	112.61(10)
M−N(3)−C(9)	110.07(6)	110.87(8)	112.55(7)

solution-state magnetic moment reported for **3** in benzene solution was 2.88 μ_B,[15e] which is very similar to the values of 2.88 and 2.68 μ_B that were observed herein for the solid-state and benzene solution magnetic moments, respectively. The ^{1}H NMR spectrum previously reported for **5** exactly matches that reported herein.[16e]

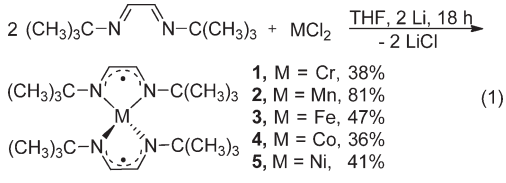

X-ray Crystal Structures of 1−5. The X-ray crystal structures of **1** and **3**−**5** were determined to establish their solid-state configurations. Despite multiple attempts, high-quality crystals of **2** could not be obtained, although a low-resolution X-ray structure revealed a monomeric, tetrahedral complex with a molecular arrangement similar to those of **3**−**5**. Experimental crystallographic data are summarized in Table 1, selected bond lengths and angles are given in Tables 2 and 3, and perspective views of **1** and **3** are presented in Figures 1 and 2. Complexes **4** and **5** are isostructural with **3**, and their perspective views are contained in the Supporting Information.

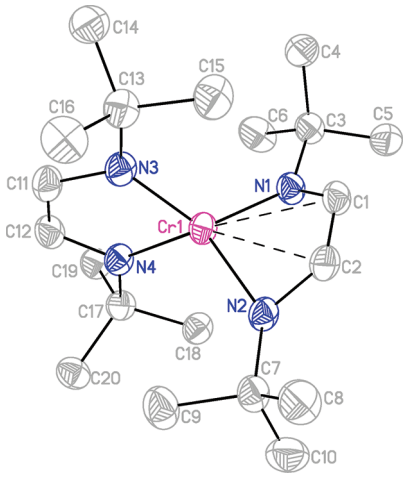

Figure 1. Perspective view of **1** with thermal ellipsoids at the 50% probability level.

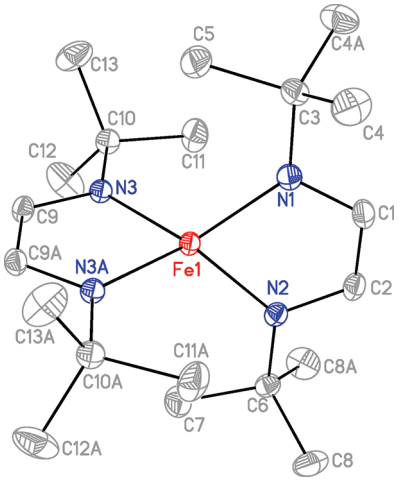

Figure 2. Perspective view of **3** with thermal ellipsoids at the 50% probability level.

Complexes **1** and **3**−**5** adopt mononuclear structures, with distorted-tetrahedral geometry about the metal centers. In **3**−**5**, the planes of the C_2N_2 ligand cores are constrained by symmetry to be orthogonal. Complex **1** crystallizes with two independent molecules in the unit cell; both molecules are identical within experimental uncertainty, and only data for the molecule containing Cr(1) are presented herein. Complexes **3**−**5** are isostructural. The metal−nitrogen bond lengths (**1**, 1.924(2)−1.934(2) Å; **3**, 1.952(1)−1.956(1) Å; **4**, 1.929(1)−1.936(1) Å; **5**, 1.916(1)−1.919 Å) fall into a narrow range. The metal−nitrogen bond distances in **1** are considerably shorter than those found in Cr(2,6-$iPr_2C_6H_3N$=CHC(Me)=NC_6H_3-2,6-iPr_2)$_2$ (2.019(1), 2.030(1) Å)[13a] and Cr(2,6-$iPr_2C_6H_3N$=CHCH=NC_6H_3-2,6-iPr_2)$_2$ (2.030(4), 2.035(5) Å)[13b] but are similar to the values observed in Cr_2(2,6-$iPr_2C_6H_3N$=CHCH=NC_6H_3-2,6-iPr_2)$_2$ (1.914(2), 1.913(2) Å).[13c] The metal−nitrogen bond distances in **3** are similar to those of Fe(C_6F_5N=C(Me)C(Me)=NC_6F_5)$_2$ (1.962(2), 1.962(2) Å)[15c] but are shorter than those found in Fe(2,6-$iPr_2C_6H_3N$=C(Me)C(Me)=NC_6H_3-2,

dx.doi.org/10.1021/om200626w |*Organometallics* 2011, 30, 5010–5017

Table 4. Sublimation Temperature, Melting Point, Solid State Decomposition Temperature, Percent Recovery, and Percent Nonvolatile Residue for 1−5

complex	sublimation temp (°C/0.05 Torr)	mp (°C)	solid-state dec temp (°C)	recovery (%)	nonvolatile residue (%)
1	85	95−97	295	96.7	3.2
2	120	155−157	325	95.0	4.3
3	115	132−134	260	96.1	3.4
4	115	174−175	235	94.7	5.2
5	115	184−185	230	92.3	6.9

6-iPr$_2$)$_2$ (1.988(9)−2.077(8) Å).[15d] Fe(C$_6$F$_5$N=C(Me)C(Me)=NC$_6$F$_5$)$_2$ is proposed to contain two diazadienyl radical anion ligands, based upon the carbon−carbon and carbon−nitrogen distances of the ligand core.[15c] In contrast, one of the ligand core carbon−carbon distances in Fe(2,6-iPr$_2$C$_6$H$_3$N=C(Me)C(Me)=NC$_6$H$_3$-2,6-iPr$_2$)$_2$ is about 0.08 Å longer than the other, suggesting more neutral character in one ligand (Chart 1, form C).[15d] The cobalt−nitrogen distances in **4** are similar to those of Co(C$_6$F$_5$N=C(Me)C(Me)=NC$_6$F$_5$)$_2$ (1.931(3), 1.932(3) Å).[16c] The nickel−nitrogen bond lengths in **5** compare well with those of Ni(C$_6$F$_5$N=C(Me)C(Me)=NC$_6$F$_5$)$_2$ (1.9173(18), 1.9165(17) Å)[16c] and Ni(2,6-Me$_2$C$_6$H$_3$N=CHC(Me)=NC$_6$H$_3$-2,6-Me$_2$)$_2$ (1.921(1)−1.948(1) Å)[16a] but are shorter than those found in Ni(2,6-iPr$_2$C$_6$H$_3$N=CHC(Me)=NC$_6$H$_3$-2,6-iPr$_2$)$_2$ (1.963(2)−1.999(2) Å).[16a] Interestingly, the X-ray crystal structure of a polymorph of **5** was reported[16d] and has nickel−nitrogen bond lengths of 1.906−1.941 Å, with an average value of 1.923 Å.

The average metal−nitrogen bond lengths follow the order **3** (1.954 Å) > **4** (1.932 Å) > **1** (1.928 Å) > **5** (1.917 Å), even though the ionic radii of the metal ions decrease in the order Cr(II) (0.80 Å) > Fe(II) (0.78 Å) > Co(II) (0.745 Å) > Ni(II) (0.69 Å).[17] Hence, the chromium−nitrogen distances in **1** are shorter than expected, on the basis of the ionic radius of the Cr(II) ion relative to those of the other ions. Closer inspection of **1** reveals that there are two types of ^{tBu2}DAD ligands. The ligand that contains N(1) and N(2) has the C(1) and C(2) atoms tilted toward the chromium atom, with chromium−carbon distances of 2.351(3) and 2.361(3) Å. In contrast, the ligand containing N(3) and N(4) forms a planar CrN$_2$C$_2$ ring and has chromium−carbon distances of 2.758 and 2.767 Å. For comparison the metal−carbon distances associated with the ^{tBu2}DAD core carbon atoms of **3**−**5** range between 2.706 and 2.727 Å and the metal ions are coplanar with the N$_2$C$_2$ rings. The chromium−carbon interactions in the ligand in **1** containing C(1) and C(2) appear to reflect the additional empty d orbitals associated with the d^4 Cr(II) ion. The modified bonding to one of the ligands in **1** may alleviate interligand *tert*-butyl crowding by a small amount, thereby allowing chromium−nitrogen bond lengths slightly shorter than expected on the basis of the ionic radius of the Cr(II) ion.

It is well-established that the carbon−carbon and carbon−nitrogen bond lengths within the C$_2$N$_2$ ligand cores offer a reliable tool for distinguishing among forms A−C in Chart 1.[13−16] In **3**−**5**, the carbon−carbon and carbon−nitrogen bond lengths fall into the narrow ranges of 1.393−1.407 and 1.326−1.347 Å, respectively. These values are between those expected for single and double bonds and are diagnostic of the ^{tBu2}DAD radical anion. These assignments are also consistent with the magnetic moment data described above. The situation with **1** is a little more complex, since one ligand has a carbon−carbon distance of 1.337(5) Å and carbon−nitrogen distances of 1.386(4) and 1.367(4) Å. The other ligand is bent toward the chromium ion and has a carbon−carbon distance of 1.395(4) Å and carbon−nitrogen distances of 1.360(4) and 1.356(4) Å. The bond distances of the latter ligand are very similar to those of **3**−**5** and support assignment as a ^{tBu2}DAD radical anion. In the former ligand, only the carbon−carbon bond length differs significantly within experimental error from that of the latter ligand. Hence, there may be a slightly higher amount of charge localization on the nitrogen atoms in the former ligand, but any differences in the structural data are small and are at the edge of experimental uncertainty. The magnetic moment data for **1** described above are consistent with the presence of two ^{tBu2}DAD radical anion ligands that are antiferromagnetically coupled to a high-spin d^4 Cr(II) ion. Complexes of the formula FeCl$_3$(^{tBu2}DAD),[18a] CoCl$_2$(^{tBu2}DAD),[18b] and NiBr$_2$(^{tBu2}DAD)[18c] have been structurally characterized and have C$_2$N$_2$ ligand core carbon−carbon and carbon−nitrogen distances of 1.455−1.510 and 1.247−1.275 Å, respectively. The carbon−carbon distances in these complexes are close to those expected for a single bond, and the carbon−nitrogen distances are close to those expected for a double bond. Hence, these ligands are consistent with neutral form C in Chart 1 and are distinct from the radical anion ligand type B observed in **1** and **3**−**5**.

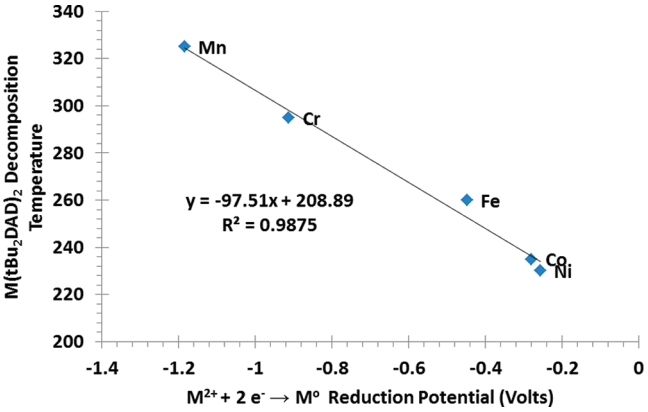

Figure 3. Comparison of the solid-state decomposition temperatures of **1**−**5** versus the M^{2+}/M^0 redox couple.

Volatility and Thermal Stability. The volatility and thermal stability of **1**−**5** were studied by preparative sublimation, thermogravimetric analyses, and melting point/solid-state thermal decomposition experiments to assess their potential for use as ALD precursors. Sublimation data, melting points, and solid-state decomposition temperatures for **1**−**5** are given in Table 4. In preparative sublimations, 0.5−1.0 g samples were sublimed at 0.05 Torr and the temperature was adjusted so that the sublimation was complete in less than 5 h. In previous work, we have established that these preparative sublimation temperatures approximate the temperatures required for the vapor phase delivery of precursors in our ALD reactors.[19] Under these conditions, the sublimed recoveries of **1**−**5** were ≥92.3% with nonvolatile residues of ≤6.9%. The high air sensitivity of **1**−**5** limited the ability to obtain higher sublimed recoveries, since product isolation had to be conducted in an inert atmosphere drybox. Additionally, exposure to trace amounts of air during

dx.doi.org/10.1021/om200626w |*Organometallics* 2011, 30, 5010–5017

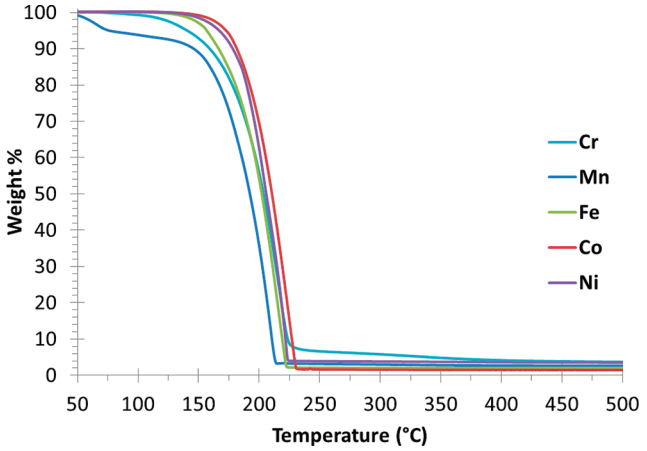

Figure 4. Thermogravimetric analysis traces of **1**−**5** from 50 to 550 °C at 10 °C/min.

sample loading may have led to higher nonvolatile residues. The solid-state decomposition temperatures were determined visually by monitoring sealed-glass capillary tubes containing a few milligrams of **1**−**5** and then noting the temperatures at which metal foils began to appear. Previous work from our growth with ALD precursors containing tris(pyrazolyl)borate or amidinate ligands has shown that solid-state decomposition temperatures are generally very close to the upper limit of self-limited ALD growth in plots of growth rate versus deposition temperature[19] and are thus very useful. The solid-state decomposition temperature of **2** is the highest at 325 °C, while that of **5** is the lowest at 230 °C. Interestingly, a plot of the solid-state decomposition temperatures of **1**−**5** versus the $M^{2+} \rightarrow M^0$ reduction potentials[20] is linear (Figure 3), suggesting that decomposition might occur through transfer of an electron from the ^{tBu2}DAD radical anion ligands to the metal ions. The failure to produce copper(II) or copper(I) complexes noted above likely arises from immediate reduction of the copper ions to copper metal, due to the large positive reduction potentials of these ions (Cu^{2+}, 0.342 V; Cu^{+}, 0.521 V).[20]

Thermogravimetric analyses (TGA) were performed on **1**−**5** to understand their volatilities and thermal stabilities (Figure 4). These analyses were carried out with an instrument that was contained in a high-purity nitrogen-filled glovebox to minimize decomposition arising from exposure to air. Complexes **1**−**5** have similar TGA traces with single-step weight losses occurring between 150 and 225 °C. The residues upon reaching 500 °C were all ≤3.6%. Complex **2** is the most air-sensitive compound in the series, and its TGA traces always showed 10−20% weight losses between 50 and 150 °C that were presumably due to reaction with ambient oxygen or water, in spite of multiple runs and utmost care to maintain a high-purity nitrogen atmosphere.

Vapor pressure measurements were carried out on **2** and **5** using a previously reported method and apparatus.[21] Details of these analyses are found in the Supporting Information. The vapor pressure of **2** obeys the equation $\log_{10} P$ (mTorr) = 12.753 − 3631/T (K), whereas the equation for **5** is $\log_{10} P$ (mTorr) = 13.983 − 3986/T (K). The vapor pressures of **2** and **5** at 115 °C are 2.48 and 5.13 Torr, respectively. The vapor pressures of **1**, **3**, and **4** should be close to those of **2** and **5**, since the preparative sublimation temperatures of **1**−**5** are similar.

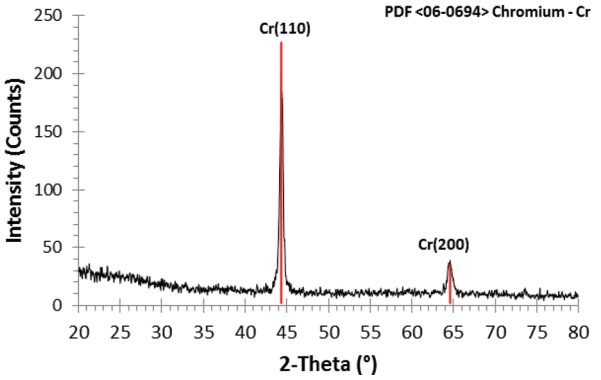

Figure 5. X-ray diffraction pattern of chromium metal powder obtained upon thermolysis of **1**.

As described above, solid-state decompositions of **1**−**5** afforded shiny metallic foils as products. To verify the formation of the metals, preparative-scale solid-state thermolyses were carried out on **1**−**5** as described in the Experimental Section and the residues were analyzed by X-ray powder diffraction. X-ray diffraction analyses demonstrated that **1** and **3**−**5** afford crystalline, shiny gray-black powders of the metals. Figure 5 shows the X-ray diffraction pattern of the chromium metal thermolysis product from **1**, which matches the JCPDS 06-0694 reference pattern for chromium metal. The X-ray diffraction patterns of the powders derived from **3**−**5** are contained in the Supporting Information. The thermolysis product of **2** was also a shiny metallic powder. The X-ray diffraction pattern of the thermolysis product obtained under conditions similar to those used for the thermolysis of **1** and **3**−**5** showed weak reflections that were consistent with Mn_3O_4 (JCPDS 04-0732).[22] Since it was possible that the Mn_3O_4 formed upon oxidation of manganese metal by residual oxygen or water in the argon used in the thermolysis experiment, the thermolysis of **2** was repeated under a vacuum of 0.05 Torr at 375 °C for 1 h. X-ray diffraction spectra of the resulting gray-black metallic powder did not show any reflections, suggesting an amorphous product. Treatment of the powders resulting from the thermolysis of **2** with 30% aqueous hydrogen peroxide led to vigorous reaction and gas evolution. Similar reactivities were observed for the powders resulting from thermolysis under flowing argon and under vacuum. For comparison, manganese metal powder reacted in a similarly vigorous manner with 30% aqueous hydrogen peroxide, whereas commercial Mn_3O_4 powder was inert under the same conditions. The commercial Mn_3O_4 powder was crystalline and indexed as Hausmannite (JCPDS 24-0734) and is thus in a different crystalline form from the powder described above that was obtained upon thermolysis of **2**. However, the reactivities of both forms of Mn_3O_4 toward 30% hydrogen peroxide should be similar. Hence, it is possible that thermolysis of **2** affords amorphous manganese metal powder.

Evaluation of Precursor Properties. Complexes **1**−**5** sublime at 85 (**1**) and 115−120 °C (**2**−**5**) with low nonvolatile residues, have high solid-state decomposition temperatures, and are highly reactive toward ambient atmosphere. Additionally, **1** and **3**−**5** decompose to the metals upon thermolysis, and **2** may afford manganese metal upon thermolysis. These complexes thus have useful properties for applications as film growth precursors by ALD and CVD. While our specific interest is in the growth of metal thin films by ALD, **1**−**5** may also be useful in the ALD and CVD growth of oxide, nitride, and other types of thin films.

Complexes **1** and **3**−**5** decompose thermally between 230 and 295 °C to afford the metals, and **2** decomposes at 325 °C possibly to afford manganese metal. Since **1**−**5** evaporate with low residues between 85 and 120 °C, they are highly likely to be useful CVD precursors to films of the metals. ALD precursors must be thermally stable at the film growth temperatures, or the self-limited ALD growth mechanism is lost and CVD-like growth occurs.[8,9] Complexes **1**−**5** also have properties that may be useful in ALD film growth, especially since they have high thermal decomposition temperatures compared to other available precursors for each metal. For example, the amidinate complex $Ni(iPrNC(Me)NiPr)_2$ decomposes at about 180 °C,[2p] in comparison to a solid-state decomposition temperature of 235 °C for nickel complex **5**. The amidinate complexes $Fe(tBuNC(Me)NtBu)_2$ and $Co(iPrNC(Me)NiPr)_2$ exhibited single-step weight loss events in the TGA traces but had 12 and 9% nonvolatile residues, respectively, upon reaching 225 ($Fe(tBuNC(Me)NtBu)_2$) and 200 °C ($Co(iPrNC(Me)NiPr)_2$).[2p] These nonvolatile residues are higher than those observed in the TGA traces of **1**−**5** (<3.6%), again suggesting that our new complexes have higher thermal decomposition temperatures than the analogous amidinate complexes. The increased thermal stabilities of **1**−**5** could allow wider temperature ranges of self-limited ALD film growth, relative to amidinate and other precursors with lower decomposition temperatures. ALD growth studies using **1**−**5** are ongoing and will be reported separately.

EXPERIMENTAL SECTION

General Considerations. All manipulations were carried out under argon using either Schlenk or glovebox techniques. Tetrahydrofuran was distilled from sodium benzophenone ketyl, and hexane was distilled from P_2O_5. Lithium metal was obtained from Acros Organics. Anhydrous transition-metal chlorides ($CrCl_2$, $MnCl_2$, $FeCl_2$, $CoCl_2$, and $NiCl_2$) were obtained from Strem Chemicals Inc. and used as received. Manganese metal powder and Mn_3O_4 were obtained from Aldrich Chemical Co. $NiCl_2 \cdot CH_3CN$[23] and 1,4-di-*tert*-butyl-1,3-diazabutadiene[24] were prepared according to literature procedures.

^1H and $^{13}C\{^1H\}$ NMR spectra were obtained at 400 and 100 MHz, respectively, in benzene-d_6 and were referenced to the residual proton and the ^{13}C resonances of the solvent. Infrared spectra were obtained using Nujol as the medium. Magnetic moments were determined in the solid state using a Johnson Mathey magnetic susceptibility apparatus and in benzene solution using the Evans method.[25] Melting points were determined on a Thermo Scientific Mel-Temp 3.0 melting point apparatus and are uncorrected. X-ray-quality crystals of **1** and **3**−**5** were grown from hexane at −23 °C. Preparative sublimations and solid-state decomposition temperatures were determined using previously described procedures.[19e] Thermogravimetric analyses were performed in a nitrogen-filled glovebox on a TA Instruments Q500 device equipped with an evolved gas analysis furnace with samples heated at a rate of 10 °C/min. Elemental analyses were performed by Midwest Microlab, Indianapolis, IN. Powder X-ray diffraction data were acquired on a Rigaku RU200B diffractometer with a Cu Kα rotating anode. Crystalline phases were identified by comparison of the experimental patterns with the powder diffraction files of the International Center of Diffraction Data using the Jade 5.0 software package.

Preparation of Bis(1,4-di-*tert*-butyl-1,3-diazabutadienyl)-chromium(II) (1). A 100 mL Schlenk flask, equipped with a magnetic stir bar and a rubber septum, was charged with 1,4-di-*tert*-butyl-1,3-diazabutadiene (1.000 g, 5.94 mmol) and tetrahydrofuran (20 mL). To this stirred solution at ambient temperature was slowly added freshly cut lithium metal (0.042 g, 6.000 mmol), and the resultant dark brown solution was stirred for 6 h. This solution was then added dropwise by cannula over a 30 min period to a stirred suspension of anhydrous chromium(II) chloride (0.365 g, 2.970 mmol) in tetrahydrofuran (40 mL). The resultant deep purple solution was stirred for 6 h at ambient temperature. The volatile components were then removed under reduced pressure, and the resultant dark purple powder was dissolved in toluene (50 mL). The solution was filtered through a 1 cm pad of Celite on a coarse glass frit, and toluene was then removed under reduced pressure. Dark purple crystals of **1** were obtained by sublimation at 85 °C/0.05 Torr (0.442 g, 38%): mp 95−97 °C; IR (Nujol, cm^{-1}) 1704 (w), 1628 (w), 1538 (w), 1246 (m), 1209 (s), 1132 (m), 1104 (m), 1034 (m); μ_{eff} = 2.83 and 2.84 μ_B in the solid state and in benzene solution, respectively. Anal. Calcd for $C_{20}H_{40}CrN_4$: C, 61.82; H, 10.38; N, 14.42. Found: C, 61.71; H, 10.06; N, 14.37.

Preparation of Bis(1,4-di-*tert*-butyl-1,3-diazabutadienyl)-manganese(II) (2). In a fashion similar to the preparation of **1**, treatment of anhydrous $MnCl_2$ (0.371 g, 2.970 mmol) in tetrahydrofuran (40 mL) with a solution of $Li^{tBu2}DAD$ (prepared from 1,4-di-*tert*-butyl-1,3-diazabutadiene (1.000 g, 5.940 mmol) and freshly cut lithium metal (0.042 g, 6.000 mmol) in tetrahydrofuran (20 mL)) for 6 h at ambient temperature afforded **2** (0.942 g, 81%) as black crystals upon sublimation at 120 °C/0.05 Torr: mp 155−157 °C; IR (Nujol, cm^{-1}) 1716 (m), 1610 (m), 1558 (w), 1364 (s), 1254 (s), 1210 (s), 1007 (m), 929 (m), 759 (s); ^1H NMR (C_6D_6, 23 °C, δ) 8.06 (s, broad, C*H*), 1.10 (s, very broad, $C(CH_3)_3$); μ_{eff} = 3.85 and 3.85 μ_B in the solid state and in benzene solution, respectively. Anal. Calcd for $C_{20}H_{40}MnN_4$: C, 61.36; H, 10.30; N, 14.31. Found: C, 60.99; H, 9.96; N, 14.01.

Preparation of Bis(1,4-di-*tert*-butyl-1,3-diazabutadienyl)-iron(II) (3). In a fashion similar to the preparation of **1**, treatment of anhydrous $FeCl_2$ (0.377 g, 2.970 mmol) in tetrahydrofuran (40 mL) with $Li^{tBu2}DAD$ (prepared from 1,4-di-*tert*-butyl-1,3-diazabutadiene (1.000 g, 5.940 mmol) and freshly cut lithium metal (0.042 g, 6.000 mmol) in tetrahydrofuran (20 mL)) for 6 h at ambient temperature afforded **3** (0.544 g, 47%) as dark brown crystals upon sublimation at 110 °C/0.05 Torr: mp 132−134 °C; IR (Nujol, cm^{-1}) 1703 (w), 1606 (w), 1525 (w), 1359 (s), 1254 (s), 1208 (s), 1022 (m), 1002 (m), 926 (m), 762 (s); μ_{eff} = 2.88 and 2.68 μ_B in the solid state and in benzene solution, respectively. Anal. Calcd for $C_{20}H_{40}FeN_4$: C, 61.22; H, 10.27; N, 14.16. Found: C, 61.39; H, 10.03; N, 14.16.

Preparation of Bis(1,4-di-*tert*-butyl-1,3-diazabutadienyl)-cobalt(II) (4). In a fashion similar to the preparation of **1**, treatment of anhydrous $CoCl_2$ (0.386 g, 2.970 mmol) in tetrahydrofuran (40 mL) with $Li^{tBu2}DAD$ (prepared from 1,4-di-*tert*-butyl-1,3-diazabutadiene (1.000 g, 5.940 mmol) and freshly cut lithium metal (0.042 g, 6.000 mmol) in tetrahydrofuran (20 mL)) for 6 h at ambient temperature afforded **4** (0.418 g, 36%) as dark blue crystals upon sublimation at 110 °C/0.05 Torr: mp 173−174 °C; IR (Nujol, cm^{-1}) 1698 (m), 1605 (m), 1527 (m), 1362 (s), 1260 (s), 1210 (s), 1008 (s), 933 (m), 763 (s); μ_{eff} = 1.75 and 1.83 μ_B in the solid state and in benzene solution, respectively. Anal. Calcd for $C_{20}H_{40}CoN_4$: C, 60.74; H, 10.19; N, 14.17. Found: C, 60.84; H, 10.01; N, 14.29.

Preparation of Bis(1,4-di-*tert*-butyl-1,3-diazabutadienyl)-nickel(II) (5). In a fashion similar to the preparation of **1**, treatment of $NiCl_2 \cdot CH_3CN$ (0.507 g, 2.970 mmol) in tetrahydrofuran (40 mL) with $Li^{tBu2}DAD$ (prepared from 1,4-di-*tert*-butyl-1,3-diazabutadiene (1.000 g, 5.940 mmol) and freshly cut lithium metal (0.042 g, 6.000 mmol) in tetrahydrofuran (20 mL)) for 6 h at ambient temperature afforded **5** (0.482 g, 41%) as dichroic red/green crystals upon sublimation at 110 °C/0.05 Torr: mp 184−185 °C; IR (Nujol, cm^{-1}) 1715 (w), 1625 (w), 1547 (w), 1493 (s), 1264 (s), 1212 (s), 934 (m), 764 (s); ^1H NMR (C_6D_6, 23 °C, δ) 8.95 (s, 2H, C*H*), 1.93 (s, 18H, $C(CH_3)_3$); $^{13}C\{^1H\}$ NMR (C_6D_6, 23 °C, ppm) 129.88 (s, CH), 64.61 (s, $C(CH_3)_3$), 30.61 (s, $C(CH_3)_3$). Anal. Calcd for $C_{20}H_{40}N_4Ni$: C, 60.77; H, 10.20; N, 14.85. Found: C, 60.89; H, 9.88; N, 14.61.

Solid-State Thermolyses of 1−5. Thermolysis experiments were performed on analytically pure samples of **1**−**5** to assess their solid-state thermal decomposition products. A 20 cm long, 2.5 cm diameter quartz tube, equipped with female 24/40 joints on each end, was fitted with two flow control valves that were attached to male 24/40 joints. A 6 cm long, 1 cm diameter glass vial was charged with 1.00 g of the sample in a glovebox. The vial was placed in the center of the quartz tube. This apparatus was placed into a tube furnace, and a 50 sccm flow of argon was established. The sample was then heated to 500 °C for 1 h and was cooled to room temperature under an argon flow. Subsequently, the powder residues were collected from the inside of the quartz tube and subjected to X-ray powder diffraction analyses as described in the text.

X-ray Crystallographic Structure Determinations. Diffraction data were measured on a Bruker X8 APEX-II κ-geometry diffractometer with Mo radiation and a graphite monochromator. Frames were collected at 100 K with the detector at 40 mm and 0.3−0.5° between each frame. The frames were recorded for 3−5 s. APEX-II[26] and SHELX[27] software were used in the collection and refinement of the models. All structures contained discrete neutral complexes without ions or solvent. Complex **1** crystallized with two independent but chemically equivalent molecules in the asymmetric unit. Complexes **3**−**5** are all isostructural, with a half-molecule in the asymmetric unit. The iron, cobalt, and nickel atoms all occupy a crystallographic mirror plane.

■ ASSOCIATED CONTENT

Supporting Information. CIF files giving X-ray crystallographic data for the structure determinations of **1** and **3**−**5** and figures giving perspective views of **4** and **5**, X-ray powder diffraction spectra of the thermolysis products of **1**−**5**, and vapor pressure determination reports for **2** and **5**. This material is available free of charge via the Internet at http://pubs.acs.org.

■ AUTHOR INFORMATION

Corresponding Author
*E-mail: chw@chem.wayne.edu.

■ ACKNOWLEDGMENT

We are grateful to the U.S. National Science Foundation (Grant No. CHE-0910475) and SAFC Hitech for support of this research.

■ REFERENCES

(1) (a) Kim, H. *Surf. Coat. Technol.* **2006**, *200*, 3104–3111. (b) Kim, H. *J. Vac. Sci. Technol. B* **2003**, *21*, 2231–2261. (c) Merchant, S. M.; Kang, S. H.; Sanganeria, M.; van Schravendijk, B.; Mountsier, T. *JOM-J. Miner. Met. Mater. Soc.* **2001**, *52*, 43–48. (d) Wang, S.-Q. *MRS Bull.* **1994**, *19*, 30–40. Roule, A.; Amuntencei, M.; Deronzier, E.; Haumesser, P. H.; Da Silva, S.; Avale, X.; Pollet, O.; Baskaran, R.; Passemard, G. *Microelectron. Eng.* **2007**, *84*, 2610–2614.

(2) (a) Waechtler, T.; Ding, S.-F.; Hofmann, L.; Mothes, R.; Xie, Q.; Oswald, S.; Detavernier, C.; Schultz, S. E.; Qu, X.-P.; Lang, H.; Gessner, T. *Microelectron. Eng.* **2011**, *88*, 684–689. (b) Moon, D.-Y.; Han, D.-S.; Shin, S.-Y.; Park, J.-W.; Kim, B. M.; Kim, J. H. *Thin Solid Films* **2011**, *519*, 3636–3640. (c) Ma, Q.; Guo, H.; Gordon, R. G.; Zaera, F. *Chem. Mater.* **2010**, *22*, 352–359. (d) Dai, M.; Kwon, J.; Halls, M. D.; Gordon, R. G.; Chabal, Y. J. *Langmuir* **2010**, *26*, 3911–3917. (e) Vidjayacoumar, B.; Emslie, D. J. H.; Clendenning, S. B.; Blackwell, J. M.; Britten, J. F.; Rheingold, A. L. *Chem. Mater.* **2010**, *22*, 4844–4853. (f) Vidjayacoumar, B.; Emslie, D. J. H.; Clendenning, S. B.; Blackwell, J. M.; Britten, J. F. *Chem. Mater.* **2010**, *22*, 4854–4866. (g) Hsu, I. J.; McCandless, B. E.; Weiland, C.; Willis, B. G. *J. Vac. Sci. Technol. A* **2009**, *27*, 660–667. (h) Lee, B. H.; Hwang, J. K.; Nam, J. W.; Lee, S. U.; Kim, J. T.; Koo, S. M.; Baunemann, A.; Fischer, R. A.; Sung, M. M. *Angew. Chem., Int. Ed.* **2009**, *48*, 4536–4539. (i) Li, Z.; Gordon, R. G. *Chem. Vap. Deposition* **2006**, *12*, 435–441. (j) Li, Z.; Rahtu, A.; Gordon, R. G. *J. Electrochem. Soc.* **2006**, *153*, C787–C794. (k) Park, K.-H.; Bradley, A. Z.; Thompson, J. S.; Marshall, W. J. *Inorg. Chem.* **2006**, *45*, 8480–8482. (l) Li, Z.; Gordon, R. G.; Farmer, D. B.; Lin, Y.; Vlassak, J. *Electrochem. Solid-State Lett.* **2005**, *8*, G182–G185. (m) Niskanen, A.; Rahtu, A.; Sajavaara, T.; Arstila, K.; Ritala, M.; Leskelä, M. *J. Electrochem. Soc.* **2005**, *152*, G25–G28. (n) Li, Z.; Barry, S. T.; Gordon, R. G. *Inorg. Chem.* **2005**, *44*, 1728–1735. (o) Lim, B. S.; Rahtu, A.; Gordon, R. G. *Nat. Mater.* **2003**, *2*, 749–754. (p) Lim, B. S.; Rahtu, A.; Park, J. S.; Gordon, R. G. *Inorg. Chem.* **2003**, *42*, 7951–7958. (q) Huo, J.; Solanki, R.; McAndrew, J. *J. Mater. Res.* **2002**, *17*, 2394–2398. (r) Solanki, R.; Pathangey, B. *Electrochem. Solid-State Lett.* **2000**, *3*, 479–480. (s) Martensson, P.; Carlsson, J.-O. *Chem. Vap. Deposition* **1997**, *3*, 45–50. (t) Juppo, M.; Ritala, M.; Leskelä, M. *J. Vac. Sci. Technol. A* **1997**, *15*, 2330–2333.

(3) (a) Haneda, M.; Iijima, J.; Koike, J. *Appl. Phys. Lett.* **2007**, *90*, 252107. (b) Usui, T.; Nasu, H.; Takahashi, S.; Shimizu, N.; Nishikawa, T.; Yoshimaru, M.; Shibata, H.; Wada, M.; Koike, J. *IEEE Trans. Electron Devices* **2006**, *52*, 2492–2499. (c) Koike, J.; Wada, M. *Appl. Phys. Lett.* **2005**, *87*, 041911.

(4) (a) Chu, J. P.; Lin, C. H.; John, V. S. *Appl. Phys. Lett.* **2007**, *91*, 132109. (b) Barmak, K.; Cabral, C., Jr.; Rodbell, K. P.; Harper, J. M. E. *J. Vac. Sci. Technol. B* **2006**, *24*, 2485–2498.

(5) (a) Lee, H.-B.-R.; Band, S.-H.; Kim, W.-H.; Gu, G. H.; Lee, Y. K.; Chung, T.-M.; Kim, C. G.; Park, C. G.; Kim, H. *Jpn. J. Appl. Phys.* **2010**, *49*, 05FA11. (b) Lee, H.-B.-R.; Gu, G. H.; Son, J. Y.; Park, C. G.; Kim, H. *Small* **2008**, *4*, 2247–2254. (c) Yang, C.-M.; Yun, S.-W.; Ha, J.-B.; Na, K.-I.; Cho, H.-I.; Lee, H.-B.; Jeong, J.-H.; Kong, S.-H.; Hahm, S.-H.; Lee, J.-H. *Jpn. J. Appl. Phys.* **2007**, *46*, 1981–1983. (d) Do, K.-W.; Yang, C.-M.; Kang, I.-S.; Kim, K.-M.; Back, K.-H.; Cho, H.-I.; Lee, H.-B.; Kong, S.-H.; Hahm, S.-H.; Kwon, D.-H.; Lee, J.-H.; Lee, J. H. *Jpn. J. Appl. Phys.* **2006**, *45*, 2975–2979. (e) Chae, J.; Park, H.-S.; Kang, S.-W. *Electrochem. Solid-State Lett.* **2002**, *5*, C64–C66.

(6) (a) Kang, S. H. *JOM* **2008**, *60*, 28–33. (b) Vaz, C. A. F.; Bland, J. A. C.; Lauhoff, G. *Rep. Prog. Phys.* **2008**, *71*, 056501. (c) Shiratsuchi, Y.; Yamamoto, M.; Bader, S. D. *Prog. Surf. Sci.* **2007**, *82*, 121–160.

(7) International Technology Roadmap for Semiconductors, http://www.itrs.net/.

(8) (a) Leskelä, M.; Ritala, M. *Angew. Chem., Int. Ed.* **2003**, *42*, 5548–5554. (b) Leskelä, M.; Ritala, M. *Thin Solid Films* **2002**, *409*, 138–146. (c) Ritala, M.; Leskelä, M. *Nanotechnology* **1999**, *10*, 19–24. (d) Niinistö, L. *Curr. Opin. Solid State Mater. Sci.* **1998**, *3*, 147–152. (e) Ritala, M. *Appl. Surf. Sci.* **1997**, *112*, 223–230. (f) Suntola, T. *Thin Solid Films* **1992**, *216*, 84–89.

(9) Putkonen, M.; Niinistö, L. *Top. Organomet. Chem.* **2005**, *9*, 125–145.

(10) (a) Kim, J.-M.; Lee, H.-B.-R.; Lansalot, C.; Dussarrat, C.; Gatineau, J.; Kim, H. *Jpn. J. Appl. Phys.* **2010**, *49*, 05FA10. (b) Li, Z.; Lee, D. K.; Coulter, M.; Rodriguez, L. N. J.; Gordon, R. G. *Dalton Trans.* **2008**, 2592–2597. (c) Lee, H.-B.-R.; Kim, H. *ECS Trans.* **2008**, *16*, 219–225. (d) Kim, K.; Lee, K.; Han, S.; Park, T.; Lee, Y.; Kim, J.; Yeom, S.; Jeon, H. *Jpn. J. Appl. Phys.* **2007**, *46*, L173–L176. Lee, K.; Kim, K.; Park, T.; Jeon, H.; Lee, Y.; Kim, J.; Yeom, S. *J. Electrochem. Soc.* **2007**, *154*, H899–H903. (e) Kim, K.; Lee, K.; Han, S.; Jeong, W.; Jeon, H. *J. Electrochem. Soc.* **2007**, *154*, H177–H181. Lee, H.-B.-R.; Kim, H. *Electrochem. Solid-State Lett.* **2006**, *9*, G323–G325.

(11) Kucheyev, S. O.; Biener, J.; Baumann, T. F.; Wang, Y. M.; Hamza, A. V.; Li, Z.; Lee, D. K.; Gordon, R. G. *Langmuir* **2008**, *24*, 943–948.

(12) Gardiner, M. G.; Hanson, G. R.; Henderson, M. J.; Lee, F. C.; Raston, C. L. *Inorg. Chem.* **1994**, *33*, 2456–2461.

(13) (a) Ghosh, M.; Sproules, S.; Weyhermüller, T.; Wieghardt, K. *Inorg. Chem.* **2008**, *47*, 5963–5970. (b) Kreisel, K. A.; Yap, G. P. A.; Theopold, K. H. *Inorg. Chem.* **2008**, *47*, 5293–5303. (c) Kreisel, K. A.; Yap, G. P. A.; Dmitrenko, O.; Landis, C. R.; Theopold, K. H. *J. Am. Chem. Soc.* **2007**, *129*, 14162–14163.

(14) Ghosh, M.; Weyhermüller, T.; Wieghardt, K. *Dalton Trans.* **2008**, 5149–5151.
(15) (a) Khusnivarov, M. M.; Weyhermüller, T.; Bill, E.; Wieghardt, K. *J. Am. Chem. Soc.* **2009**, *131*, 1208–1221. (b) Khusnivarov, M. M.; Weyhermüller, T.; Bill, E.; Wieghardt, K. *Angew. Chem., Int. Ed.* **2008**, *47*, 1228–1231. (c) Muresan, N.; Lu, C. C.; Ghosh, M.; Peters, J. C.; Abe, M.; Henling, L. M.; Weyhermöller, T.; Bill, E.; Wieghardt, K. *Inorg. Chem.* **2008**, *47*, 4579–4590. (d) Bart, S. C.; Hawrelak, E. J.; Lobkovsky, E.; Chirik, P. J. *Organometallics* **2005**, *24*, 5518–5527. (e) tom Dieck, H.; Diercks, R.; Stamp, L.; Bruder, H.; Schuld, T. *Chem. Ber.* **1987**, *120*, 1943–1950. (f) tom Dieck, H.; Bruder, H. *J. Chem. Soc., Chem. Commun.* **1977**, 24–25.
(16) (a) Muresan, N.; Weyhermüller, T.; Wieghardt, K. *Dalton Trans.* **2007**, 4390–4398. (b) Muresan, N.; Chlopek, K.; Weyhermüller, T.; Neese, F.; Wieghardt, K. *Inorg. Chem.* **2007**, *46*, 5327–5337. (c) Khusnivarov, M. M.; Harms, K.; Burghaus, O.; Sundermeyer, J. *Eur. J. Inorg. Chem.* **2006**, 2985–2996. (d) Gorls, H.; Walther, D.; Sieler, J. *Cryst. Res. Technol.* **1987**, *22*, 1145–1151. (e) Svoboda, M.; tom Dieck, H.; Kruger, C.; Tsay, Y.-H. *Z. Naturforsch.* **1981**, *36b*, 814–822. (f) Robinson, M. A.; Curry, J. D.; Busch, D. H. *Inorg. Chem.* **1963**, *2*, 1178–1181. (g) Kaltsoyannis, N. *J. Chem. Soc., Dalton Trans.* **1996**, 1583–1589.
(17) Greenwood, N. N.; Earnshaw, A. *Chemistry of the Elements*, 2nd ed.; Butterworth-Heinemann: Oxford, U.K., 1997; pp 1004, 1074, 1115, 1148.
(18) (a) Allan, L. E. N.; Shaver, M. P.; White, A. J. P.; Gibson, V. C. *Inorg. Chem.* **2007**, *46*, 8963–8970. (b) Barral, M. C.; Delgado, E.; Gutíerrez-Puebla, E.; Jimenez-Aparicio, R.; Monge, A.; del Pino, C.; Santos, A. *Inorg. Chim. Acta* **1983**, *74*, 101–107. (c) Jameson, G. B.; Oswald, H. R.; Beer, H. R. *J. Am. Chem. Soc.* **1984**, *106*, 1669–1675.
(19) (a) Saly, M. J.; Munnik, F.; Winter, C. H. *J. Mater. Chem.* **2010**, *20*, 9995–10000. (b) Saly, M. J.; Munnik, F.; Baird, R. J.; Winter, C. H. *Chem. Mater.* **2009**, *21*, 3742–3744. (c) Saly, M. J.; Munnik, F.; Winter, C. H. *Chem. Vap. Deposition* **2011**, *17*, 128–134. (d) Wiedmann, M. K.; Karunarathne, M. C.; Baird, R. J.; Winter, C. H. *Chem. Mater.* **2010**, *22*, 4400–4405. (e) Saly, M. J.; Heeg, M. J.; Winter, C. H. *Inorg. Chem.* **2009**, *48*, 5303–5312. (f) Wiedmann, M. K.; Heeg, M. J.; Winter, C. H. *Inorg. Chem.* **2009**, *48*, 5382–5391.
(20) *CRC Handbook of Chemistry and Physics*, 91st ed.; CRC Press: Boca Raton, FL, 2010−2011; pp 8-20, 8-29.
(21) Rushworth, S. A.; Smith, L. M.; Kingsley, A. J.; Odedra, R.; Nickson, R.; Hughes, P. *Microelectron. Reliab.* **2005**, *45*, 1000–1002.
(22) Xu, H. Y.; Xu, S. L.; Wang, H.; Yan, H. *J. Electrochem. Soc.* **2005**, *152*, C803–C807.
(23) Reedijk, J.; Groeneveld, W. L. *Recl. Trav. Chim. Pays-Bas* **1968**, *87*, 552–558.
(24) Kliegman, J. M.; Barnes, R. K. *Tetrahedron* **1970**, *26*, 2555–2560.
(25) Evans, D. F. *J. Chem. Soc.* **1959**, 2003.
(26) APEX II collection and processing programs are distributed by the manufacturer, Bruker AXS Inc., Madison, WI, 2009.
(27) Sheldrick, G. M. *Acta Crystallogr., Sect. A: Found. Crystallogr.* **2008**, *64*, 112–122.